Combustion Theory and Modelling
Publication details, including instructions for authors and subscription information:
http://www.tandfonline.com/loi/tctm20

An accurate method to implement boundary conditions for reacting flows based on characteristic wave analysis

Watit Pakdee [a] & Shankar Mahalingam [b]

[a] Department of Mechanical Engineering, University of Colorado at Boulder, Boulder, CO, 80309, USA

[b] Department of Mechanical Engineering, University of California, Riverside, CA, 92521, USA

Available online: 29 Jul 2009

To cite this article: Watit Pakdee & Shankar Mahalingam (2003): An accurate method to implement boundary conditions for reacting flows based on characteristic wave analysis, Combustion Theory and Modelling, 7:4, 705-729

To link to this article: http://dx.doi.org/10.1088/1364-7830/7/4/006

INSTITUTE OF PHYSICS PUBLISHING COMBUSTION THEORY AND MODELLING

Combust. Theory Modelling **7** (2003) 705–729 PII: S1364-7830(03)63034-2

An accurate method to implement boundary conditions for reacting flows based on characteristic wave analysis

Watit Pakdee[1] **and Shankar Mahalingam**[2,3]

[1] Department of Mechanical Engineering, University of Colorado at Boulder, Boulder, CO 80309, USA
[2] Department of Mechanical Engineering, University of California, Riverside, CA 92521, USA

E-mail: shankar.mahalingam@ucr.edu

Received 2 May 2003, in final form 9 September 2003
Published 24 October 2003
Online at stacks.iop.org/CTM/7/705

Abstract

A characteristic wave analysis previously developed to specify boundary conditions for chemically reacting flows with realistic thermodynamic properties is derived with an alternative set of primitive variables. In a multicomponent reacting flow, it is sufficient to consider the time-integration of all species' mass fractions, excluding one. This results in a primitive variables vector that contains one element less. The impact of this choice on the resulting characteristic equations and treatment of numerical boundary conditions are presented. The improved accuracy in the treatment of boundary conditions is assessed via three test problems including non-reacting and reacting situations. The method presented is found to provide accurate results as it allows acoustic waves, pressure waves and vortices to propagate through the domain without discernible reflection. Furthermore, the method eliminates the drift of the mean pressure that tends to occur over long integration times when the boundary is treated inaccurately.

1. Introduction

Methods to implement boundary conditions for numerical solutions of Navier–Stokes equations in chemically reacting flows have been of interest in a number of recent studies. Algorithms based on high-order schemes can provide spectral-like resolution and allow very low numerical dissipation [1–3]. However, their potential application would be constrained to only periodic boundary conditions if boundary treatment to impose general physical boundary conditions is not precise. Poinsot and Lele [4] defined a boundary condition as a numerical boundary condition when no dependent variable is explicitly imposed at the boundary. In such situations,

[3] Author to whom any correspondence should be addressed.

the number of physical boundary conditions is smaller than the number of primitive variables. Numerical boundary conditions are then needed to solve the problem numerically [4]. These boundary conditions are required to prevent spurious wave reflection at the boundaries. Thompson [5] developed a formulation to treat boundary conditions for systems of hyperbolic equations, such as Euler equations, using characteristic theory in which the different waves moving across boundaries are analysed. Extensive studies of this characteristic wave analysis have been conducted for Euler equations [1, 2, 6–8]. Based on this analysis Poinsot and Lele [4] developed a method called Navier–Stokes characteristic boundary conditions (NSCBCs) specifically for the Navier–Stokes equations. The main concept is based on the characteristic property of hyperbolic systems coupled with the idea that Navier–Stokes equations reduce to Euler equations when the viscous terms are set to zero. Baum *et al* [9] subsequently extended the NSCBC method to multicomponent reactive flows. All the derivations described above were based on perfect gas flows. Further extension of the method has been presented by Okong'o and Bellan [10] for real gas mixtures.

To implement the characteristic method, vectors of conservative and primitive variables are first determined. The choice of the set of primitive variable vector depends on practical applications or problems of interest. Baum *et al* [9] used density ρ, temperature T, velocity components u_1, u_2, u_3, and species mass fractions $Y_1, Y_1, \ldots, Y_N$ for perfect gas with inhomogeneous, variable thermodynamic properties. In this paper, instead of temperature T, we propose to use pressure p as a primitive variable. This requires modification of the characteristic analysis that is considered in this work.

First, we consider the primitive variable vector $U = (\rho, p, u_1, u_2, u_3, Y_1, Y_2, \ldots, Y_N)$ that includes all N species in the reacting flow mixture. The NSCBC method is derived and results are similar to [9], with differences directly attributable to the different choice of the primitive variable vector. In a multicomponent reacting flow, noting that the sum of the mass fractions is unity, it is sufficient to consider the time-advancement of all species mass fractions, excluding one. Often, nitrogen, N_2, appears in excess and its mass fraction is not computed explicitly. Instead, it is obtained via the constraint that the sum of mass fractions is unity. In this paper, for convenience, the Nth species is taken to be N_2. This choice results in a primitive variable vector that contains one element less, namely, Y_N. Consequently, the NSCBC method requires modification. This forms the focus of this paper. We evaluate the performance of the NSCBC method that ignores this subtlety against the modified method to demonstrate resulting inaccuracies in the computed solution.

Section 2 presents the alternative method derived for the chosen primitive variables for the fully compressible, chemically reacting, Navier–Stokes equations. The section also describes modification to the formulation to take into account the case in which Y_{N_2} is excluded and computed separately. A detailed mathematical derivation of the method appears in the appendix. Procedures to implement boundary conditions are described in section 3. In section 4, the performance of the method is assessed using test problems. Concluding remarks are given in section 5.

2. Mathematical formulation

2.1. Characteristic form of Navier–Stokes equations

The system of governing equations includes continuity, Navier–Stokes, energy and species equations. This system of equations written in tensor form is

$$\frac{\partial \rho}{\partial t} + \frac{\partial (\rho u_j)}{\partial x_j} = 0, \tag{2.1}$$

$$\frac{\partial \rho u_i}{\partial t} + \frac{\partial (\rho u_i u_j)}{\partial x_j} = -\frac{\partial p}{\partial x_i} + \frac{\partial \tau_{ij}}{\partial x_j}, \tag{2.2}$$

$$\frac{\partial \rho e_t}{\partial t} + \frac{\partial [(\rho e_t + p) u_j]}{\partial x_j} = \frac{\partial}{\partial x_i}(u_j \tau_{ij}) - \frac{\partial q_j}{\partial x_j}, \tag{2.3}$$

$$\frac{\partial \rho Y_\kappa}{\partial t} + \frac{\partial (\rho Y_\kappa u_j)}{\partial x_j} = -\frac{\partial (\rho Y_\kappa V_{\kappa j})}{\partial x_j} + \dot{\omega}_\kappa, \qquad \kappa = 1, \ldots, N, \tag{2.4}$$

where u_j denotes the jth velocity component along spatial coordinate x_j and t is time. The mass production rate of the κth species is denoted by $\dot{\omega}_\kappa$. The stress tensor, heat flux vector and diffusion velocities are given, respectively, by

$$\tau_{ij} = \mu \left(\frac{\partial u_i}{\partial x_j} + \frac{\partial u_j}{\partial x_i} - \frac{2}{3} \delta_{ij} \frac{\partial u_k}{\partial x_k} \right), \tag{2.5}$$

$$q_j = -\lambda \frac{\partial T}{\partial x_j} + \rho \sum_{\kappa=1}^{N} h_\kappa Y_\kappa V_{\kappa j}, \tag{2.6}$$

$$V_{\kappa j} = -\mathcal{D}_\kappa \frac{1}{Y_\kappa} \frac{\partial Y_\kappa}{\partial x_j}, \qquad \kappa = 1, 2, \ldots, N, \tag{2.7}$$

where $\mathcal{D}_\kappa$ is the diffusion coefficient of species κ, λ and μ are the mixture thermal conductivity and viscosity, respectively. The quantity e_t is the total energy per unit mass of the mixture,

$$e_t = e + \frac{1}{2} \sum_{k=1}^{3} u_k^2, \qquad e = \sum_{\kappa=1}^{N} Y_\kappa h_\kappa - \frac{p}{\rho}, \tag{2.8}$$

where e is the internal energy per unit mass and h_κ is the enthalpy of species κ given by

$$h_\kappa = h_\kappa^0 + \int_{T_0}^{T} C_{p\kappa}(T')\, \mathrm{d}T', \qquad \kappa = 1, \ldots, N, \tag{2.9}$$

where h_κ^0 and $C_{p\kappa}$ denote the enthalpy of formation and specific heat of species κ. The mixture specific heat is given by

$$\bar{C}_p(T) = \sum_{\kappa=1}^{N} Y_\kappa C_{p\kappa}(T). \tag{2.10}$$

Pressure, density and temperature are related through the ideal gas equation of state

$$p = \rho R T, \tag{2.11}$$

where R is the reacting mixture gas constant given by

$$R = \frac{\Re}{\bar{W}}, \qquad \bar{W} = \left[\sum_{\kappa=1}^{N} \left(\frac{Y_\kappa}{W_\kappa} \right) \right]^{-1}, \tag{2.12}$$

where $\Re$ is the universal gas constant, $\bar{W}$ is the average molecular weight of the mixture, and W_κ is the species molecular weight. Note that R is not a constant, but a function of the local reacting gas mixture composition.

Next, the hyperbolic portion of the system of governing equations is partly rewritten in characteristic form in which characteristic waves in the x_1 direction are easily identified.

The detailed mathematical derivation is contained in the appendix. We write the system of equations in primitive form as given by (A.10). From the derivation we obtain

$$\frac{\partial U}{\partial t} + S\mathcal{L} + C = 0,$$

where the values of $\mathcal{L}_i$ can be obtained by (A.11) as follows:

$$\mathcal{L}_1 = (u_1 - c)\left(\frac{\partial p}{\partial x_1} - \rho c \frac{\partial u_1}{\partial x_1}\right), \tag{2.13}$$

$$\mathcal{L}_2 = u_1\left(c^2 \frac{\partial \rho}{\partial x_1} - \frac{\partial p}{\partial x_1}\right), \tag{2.14}$$

$$\mathcal{L}_3 = u_1\left(\frac{\partial u_2}{\partial x_1}\right), \tag{2.15}$$

$$\mathcal{L}_4 = u_1\left(\frac{\partial u_3}{\partial x_1}\right), \tag{2.16}$$

$$\mathcal{L}_5 = (u_1 + c)\left(\frac{\partial p}{\partial x_1} + \rho c \frac{\partial u_1}{\partial x_1}\right), \tag{2.17}$$

$$\mathcal{L}_{\kappa+5} = u_1 \frac{\partial Y_\kappa}{\partial x_1}, \qquad \kappa = 1, 2, \ldots, N, \tag{2.18}$$

where c is the reacting mixture sound speed given by (A.29).

Defining vector $\boldsymbol{d} = S\mathcal{L}$, which is $A^1(\partial U/\partial x_1)$ appearing, respectively, in (A.8) and (A.10):

$$\boldsymbol{d} = \begin{bmatrix} d_1 \\ d_2 \\ d_3 \\ d_4 \\ d_5 \\ d_6 \\ \vdots \\ d_{N+5} \end{bmatrix} \equiv S\mathcal{L} = \begin{bmatrix} \frac{1}{c^2}\left(\mathcal{L}_2 + \frac{\mathcal{L}_1 + \mathcal{L}_5}{2}\right) \\ \frac{\mathcal{L}_1 + \mathcal{L}_5}{2} \\ \frac{\mathcal{L}_5 - \mathcal{L}_1}{2\rho c} \\ \mathcal{L}_3 \\ \mathcal{L}_4 \\ \mathcal{L}_6 \\ \vdots \\ \mathcal{L}_{N+5} \end{bmatrix}. \tag{2.19}$$

As given in (A.12) in terms of conservative form, we may now write the system of equations in terms of $\boldsymbol{d}$ as

$$\frac{\partial \tilde{U}}{\partial t} + P\boldsymbol{d} + \tilde{C} = 0,$$

where vector $P\boldsymbol{d}$ can be expressed as

$$P\boldsymbol{d} = \begin{bmatrix} d_1 \\ (P\boldsymbol{d})_{2,1} \\ u_1 d_1 + \rho d_3 \\ u_2 d_1 + \rho d_4 \\ u_3 d_1 + \rho d_5 \\ Y_1 d_1 + \rho d_6 \\ Y_2 d_1 + \rho d_7 \\ \vdots \\ Y_N d_1 + \rho d_{N+5} \end{bmatrix}, \tag{2.20}$$

where

$$(P\boldsymbol{d})_{2,1} = \left(\frac{1}{2}u_k u_k + \sum_{\kappa=1}^{N} Y_\kappa h_\kappa - \bar{C}_p T\right) d_1 + \left(\frac{\bar{C}_p - R}{R}\right) d_2 + \rho u_1 d_3 + \rho u_2 d_4 + \rho u_3 d_5 + \sum_{\kappa=1}^{N} \left(\rho h_\kappa - p\frac{\bar{W}}{W_\kappa}\frac{\bar{C}_p}{R}\right) d_{\kappa+5}. \tag{2.21}$$

The energy equation (2.3), with the characteristic term $(P\boldsymbol{d})_{2,1}$ replacing the flux term in the x_1 direction, becomes

$$\frac{\partial \rho e_t}{\partial t} + (P\boldsymbol{d})_{2,1} + \frac{\partial[(\rho e_t + p)u_2]}{\partial x_2} + \frac{\partial[(\rho e_t + p)u_3]}{\partial x_3} = \frac{\partial(u_j \tau_{ij})}{\partial x_i} - \frac{\partial q_j}{\partial x_j}. \tag{2.22}$$

If one chooses to compute only $(N-1)$ mass fractions, it is tempting to write down

$$(P\boldsymbol{d})_{2,1} = \left(\frac{1}{2}u_k u_k + \sum_{\kappa=1}^{N} Y_\kappa h_\kappa - \bar{C}_p T\right) d_1 + \left(\frac{\bar{C}_p - R}{R}\right) d_2 + \rho u_1 d_3 + \rho u_2 d_4 + \rho u_3 d_5 + \sum_{\kappa=1}^{N-1} \left(\rho h_\kappa - p\frac{\bar{W}}{W_\kappa}\frac{\bar{C}_p}{R}\right) d_{\kappa+5}, \tag{2.23}$$

where the last summation term ranges from 1 to $N-1$. However, this procedure is incorrect since it ignores the new set of primitive variables implied. Equation (2.23) is the incorrect expression of $(P\boldsymbol{d})_{2,1}$ leading to an incorrect boundary formulation. If we exclude N_2 from the time-advancement process and instead compute Y_{N_2} using

$$Y_{N_2} = 1 - \sum_{\kappa=1}^{N-1} Y_\kappa, \tag{2.24}$$

then it implies that the primitive variable vector is no longer given by (A.15). The new vector is

$$U = (\rho, p, u_1, u_2, u_3, Y_1, \ldots, Y_{N-1})^{\mathrm{T}}. \tag{2.25}$$

The conservative variable vector and the flux vector become, respectively,

$$\tilde{U} = (\rho, \rho e_t, \rho u_1, \rho u_2, \rho u_3, \rho Y_1, \ldots, \rho Y_{N-1})^{\mathrm{T}}, \tag{2.26}$$

$$F^1 = (\rho u_1, (\rho e_t + p)u_1, \rho u_1^2 + p, \rho u_1 u_2, \rho u_1 u_3, \rho u_1 Y_1, \ldots, \rho u_1 Y_{N-1})^{\mathrm{T}}. \tag{2.27}$$

Including the Y_{N_2} contribution, the total energy e may be rewritten as

$$e = \sum_{\kappa=1}^{N-1} Y_\kappa h_\kappa + Y_{N_2} h_{N_2} - \frac{p}{\rho} + \frac{1}{2}\sum_{k=1}^{3} u_k^2. \tag{2.28}$$

Consequently, the terms associated with the derivatives of e with respect to Y_κ are modified as

$$P_{2,\kappa+5} = \rho(h_\kappa - h_{N_2}) - \sum_{\kappa'=1}^{N-1} p\bar{W}\left(\frac{1}{W_\kappa} - \frac{1}{W_{N_2}}\right) Y_{\kappa'} \frac{C_{p,\kappa'}}{R}, \tag{2.29}$$

$$Q^1_{2,\kappa+5} = u_1\left(\rho(h_\kappa - h_{N_2}) - \sum_{\kappa'=1}^{N-1} p\bar{W}\left(\frac{1}{W_\kappa} - \frac{1}{W_{N_2}}\right) Y_{\kappa'} \frac{C_{p,\kappa'}}{R}\right), \tag{2.30}$$

where $\kappa = 1, \ldots, N-1$.

Similarly, by following the lines of derivation presented in this paper, the correct form of $(P\boldsymbol{d})_{2,1}$ associated with the characteristic form of the energy conservation equation is finally deduced to be

$$(P\boldsymbol{d})_{2,1} = \left(\frac{1}{2}u_k u_k + \sum_{\kappa=1}^{N} Y_\kappa h_\kappa - \bar{C}_p T\right) d_1 + \left(\frac{\bar{C}_p - R}{R}\right) d_2 + \rho u_1 d_3 + \rho u_2 d_4 + \rho u_3 d_5 + \sum_{\kappa=1}^{N-1}\left[\rho(h_\kappa - h_{\mathrm{N}_2}) - p\bar{W}\frac{\bar{C}_p}{R}\left(\frac{1}{W_\kappa} - \frac{1}{W_{\mathrm{N}_2}}\right)\right] d_{\kappa+5}. \tag{2.31}$$

Note from the last term of the above equation, since $d_{\kappa+5} = u_1 \partial Y_\kappa / \partial x_1$, inaccuracies do not occur when the mass fraction gradients and/or velocity at the boundary is zero. Thus, to test the formulation, we examine problems in which the mass fraction gradients at the boundaries are necessarily non-zero. Further comments pertaining to this issue appear in section 4.

2.2. *Characteristic wave specification*

The approach used to specify the values of characteristic wave $\mathcal{L}_i$ for multidimensional Navier–Stokes equations was introduced by Poinsot and Lele [4]. Wave amplitudes at the boundaries are determined by examining a locally one-dimensional inviscid (LODI) non-reacting problem. Values of $\mathcal{L}_i$ can be specified for chosen boundary conditions based on the LODI relations. The LODI system is readily obtained by considering the primitive system of equations (A.12) and neglecting viscous, reactive and transverse terms. The resulting equations (LODI relations) are

$$\frac{\partial \rho}{\partial t} + \frac{1}{c^2}\left(\mathcal{L}_2 + \frac{\mathcal{L}_1 + \mathcal{L}_5}{2}\right) = 0, \tag{2.32}$$

$$\frac{\partial p}{\partial t} + \frac{\mathcal{L}_1 + \mathcal{L}_5}{2} = 0, \tag{2.33}$$

$$\frac{\partial u_1}{\partial t} + \frac{\mathcal{L}_5 - \mathcal{L}_1}{2\rho c} = 0, \tag{2.34}$$

$$\frac{\partial u_2}{\partial t} + \mathcal{L}_3 = 0, \tag{2.35}$$

$$\frac{\partial u_3}{\partial t} + \mathcal{L}_4 = 0, \tag{2.36}$$

$$\frac{\partial Y_\kappa}{\partial t} + \mathcal{L}_{\kappa+5} = 0, \qquad \kappa = 1, 2, \ldots, N. \tag{2.37}$$

The time derivative of temperature can be computed by using the above relations and can be written as

$$\frac{\partial T}{\partial t} - \frac{T}{c^2\rho}\left[\frac{1-\gamma}{2}(\mathcal{L}_1 + \mathcal{L}_5) + \mathcal{L}_2\right] - T\bar{W}\sum_{\kappa=1}^{N}\frac{\mathcal{L}_{\kappa+5}}{W_\kappa} = 0. \tag{2.38}$$

By inverting the definitions of characteristic waves, $\mathcal{L}_i^{'s}$ (equations (2.13)–(2.18)), the LODI relations in terms of gradients are

$$\frac{\partial \rho}{\partial x_1} = \frac{1}{c^2}\left(\frac{\mathcal{L}_2}{u_1} + \frac{1}{2}\left(\frac{\mathcal{L}_5}{u_1 + c} + \frac{\mathcal{L}_1}{u_1 - c}\right)\right), \tag{2.39}$$

$$\frac{\partial p}{\partial x_1} = \frac{1}{2}\left(\frac{\mathcal{L}_5}{u_1 + c} + \frac{\mathcal{L}_1}{u_1 - c}\right), \tag{2.40}$$

$$\frac{\partial u_1}{\partial x_1} = \frac{1}{2\rho c}\left(\frac{\mathcal{L}_5}{u_1 + c} - \frac{\mathcal{L}_1}{u_1 - c}\right), \tag{2.41}$$

$$\frac{\partial u_2}{\partial x_1} = \frac{\mathcal{L}_3}{u_1}, \tag{2.42}$$

$$\frac{\partial u_3}{\partial x_1} = \frac{\mathcal{L}_4}{u_1}, \tag{2.43}$$

$$\frac{\partial Y_\kappa}{\partial x_1} = \frac{\mathcal{L}_{\kappa+5}}{u_1}, \qquad \kappa = 1, 2, \ldots, N. \tag{2.44}$$

Using the above definitions along with the equation of state, $\partial T/\partial x_1$ can be expressed by

$$\frac{\partial T}{\partial x_1} = \frac{T}{c^2\rho}\left[\frac{\gamma-1}{2}\left(\frac{\mathcal{L}_5}{u_1+c} + \frac{\mathcal{L}_1}{u_1-c}\right) - \frac{\mathcal{L}_2}{u_1}\right] - \frac{T\bar{W}}{u_1}\sum_{\kappa=1}^{N}\mathcal{L}_{\kappa+5}. \tag{2.45}$$

3. Implementation of boundary conditions

The procedure to implement boundary conditions involves three principal steps.

1. Distinguish the incoming and the outgoing waves on the boundary by determining the sign of eigenvalues associated with different $\mathcal{L}_i$. The number of incoming waves determines the number of physical boundary conditions needed in order for the problem to be well-posed. The conservation equations associated with each physical boundary imposed are eliminated.
2. The outgoing waves can be computed from the information inside the domain. The incoming waves are expressed as a function of the known outgoing waves by using the appropriate LODI relations.
3. Combine the remaining conservation equations with the specified $\mathcal{L}_i$ obtained from step 2 to compute all variables that were not given by physical boundary conditions. The system of equations is now ready for time integration.

A non-reflecting boundary condition is considered on both lateral boundaries. At the right boundary, all the $\mathcal{L}_i$ but $\mathcal{L}_1$ are outgoing waves. The characteristic wave amplitudes associated with the outgoing waves can be computed from solution at interior points and given by equations (2.14)–(2.18). On the other hand, the boundary condition associated with the incoming wave $\mathcal{L}_1$ is needed. Imposing any one physical boundary condition for the primitive variables would lead to a well-posed problem [4]. Oliger and Sundström [11] specified constant pressure at the outlet boundary to ensure well-posedness. However, this technique generates acoustic wave reflection at the outlet. To avoid this numerical reflection, $\mathcal{L}_1 = 0$ may be considered. However, with this condition, the information on mean pressure that is conveyed by wave reflection can never be fed back into the computational domain leading to an ill-posed problem [4]. Due to this problem, we may let small wave reflections back into the domain. As a result, $\mathcal{L}_1$ is defined as [4, 12, 13]

$$\mathcal{L}_1 = K(p - p_\infty), \tag{3.1}$$

where K is a constant chosen as recommended in [4].

In the case of the left boundary, $\mathcal{L}_1$ associated with negative eigenvalue (u_1–c) is the only outgoing wave. Therefore, this characteristic wave amplitude can be computed from solution at interior points and given by (2.13). All other characteristic wave amplitudes are set to zero.

4. Tests of formulation

The compressible direct simulation code [14] originally developed for computation of perfect gases with constant specific heats was modified appropriately for this work. Simple Fickian

diffusion is used to model transport and the Lewis number approximation recommended by Smooke and Giovangigli [15] is employed. Spatial derivatives are discretized using a sixth-order accurate compact finite difference scheme [2]. A third-order Runge–Kutta scheme is used to integrate the evolution equations in time.

Three test problems are discussed in the following subsections. Two cases are considered. In both cases, Y_{N_2} is computed via (2.24) and thus its evolution equation is not considered. In case I, the boundaries are treated by correctly accounting for the implied primitive variable vector, whereas in case II the boundaries are treated inaccurately via (2.23). Considering (2.31), as addressed earlier, the term contributing Y_{N_2} effects will vanish when gradients of all the species are zero. Therefore, to distinguish between case I and case II, we set non-zero gradients of initial mass fractions at the boundaries. In the third problem, the boundary condition corresponding to case I is applied to the study of the interaction of a pair of counter-rotating vortices with a premixed flame. This represents a chemically reacting flow problem unlike the first two test problems.

In most situations, computational domains are chosen so that no significant activity occurs at the boundary. However, in problems involving convection of a structure within which significant chemical activity could be occurring, non-zero mass fraction gradients will develop as the structure exits the computational boundary. This situation occurs, for instance, in a flame/vortex interaction problem that has been extensively investigated. A review of studies on this problem can be found in [17]. Even if significant chemical reaction has ceased as the vortex exits the domain, the physical structure of the vortex could lead to mass fraction gradients arising in the direction of vortex propagation. Inaccurate treatment of the boundary could lead to errors as demonstrated through test problems presented in this section.

4.1. One-dimensional acoustic wave propagation

A one-dimensional problem involving acoustic wave propagation towards a non-reflecting boundary is simulated. The acoustic wave is generated using the following initial conditions [9]:

$$\begin{aligned} u &= u_0 + A \exp\left[-\left(B \frac{x - L/2}{L} \right)^2 \right], \\ p &= p_0 + \rho_0 c_0 (u - u_0), \\ \rho &= \rho_0 + \frac{\rho (u - u_0)}{c_0}, \\ T &= \frac{p}{\rho R}, \end{aligned} \tag{4.1}$$

where subscript 0 represents reference quantities. Reference pressure p_0 is 101 325 N m^{-2}. The reference speed of sound c_0 and density ρ_0 correspond to the quantities based on initial values at the left boundary. The computed values of c_0 and ρ_0 are 818.74 m s^{-1} and 0.227 kg m^{-3}, respectively. Constants $A = 8$ m s^{-1} and $B = 5$ indicate, respectively, the strength and the stiffness of the acoustic wave. The width of velocity profile L is one-third of the domain length in the x direction. The mixture field includes CH_4, O_2, CO_2, CO, H_2, H_2O, H, and N_2. The mass fractions of these species are initialized as shown in figure 1(*a*). A subsonic non-reflecting boundary condition is implemented on both left and right boundaries. We set 129 points in the x direction over the 5.4 mm domain.

The velocity and the pressure corresponding to acoustic wave propagation moving to the right of the domain for case I are shown in figures 2 and 3, respectively. Results at a different value of a reduced time $t_r = 2c_0 t/L$ are shown. It can be seen that the acoustic wave exits the

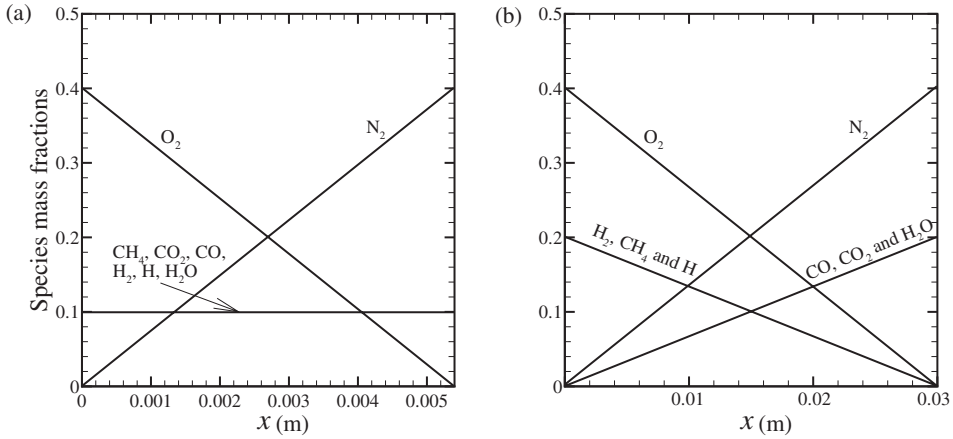

Figure 1. Initial profiles of mass fractions for two test problems: (*a*) one-dimensional and (*b*) two-dimensional cases.

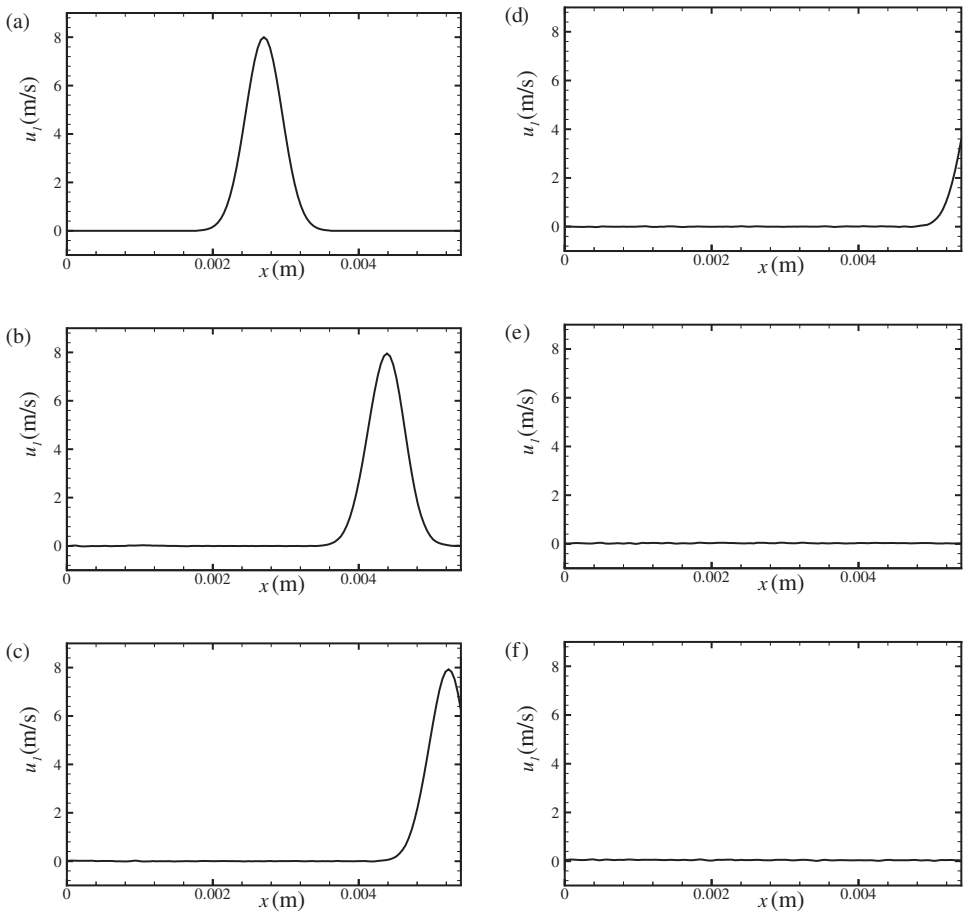

Figure 2. Velocity wave propagation ($\mathrm{m\,s^{-1}}$) for case I. In all cases, the scale on the y-axis is unchanged to facilitate direct comparison. (*a*) $t_r = 0.0$, (*b*) $t_r = 0.427$, (*c*) $t_r = 0.855$, (*d*) $t_r = 1.068$, (*e*) $t_r = 6.471$, (*f*) $t_r = 12.957$.

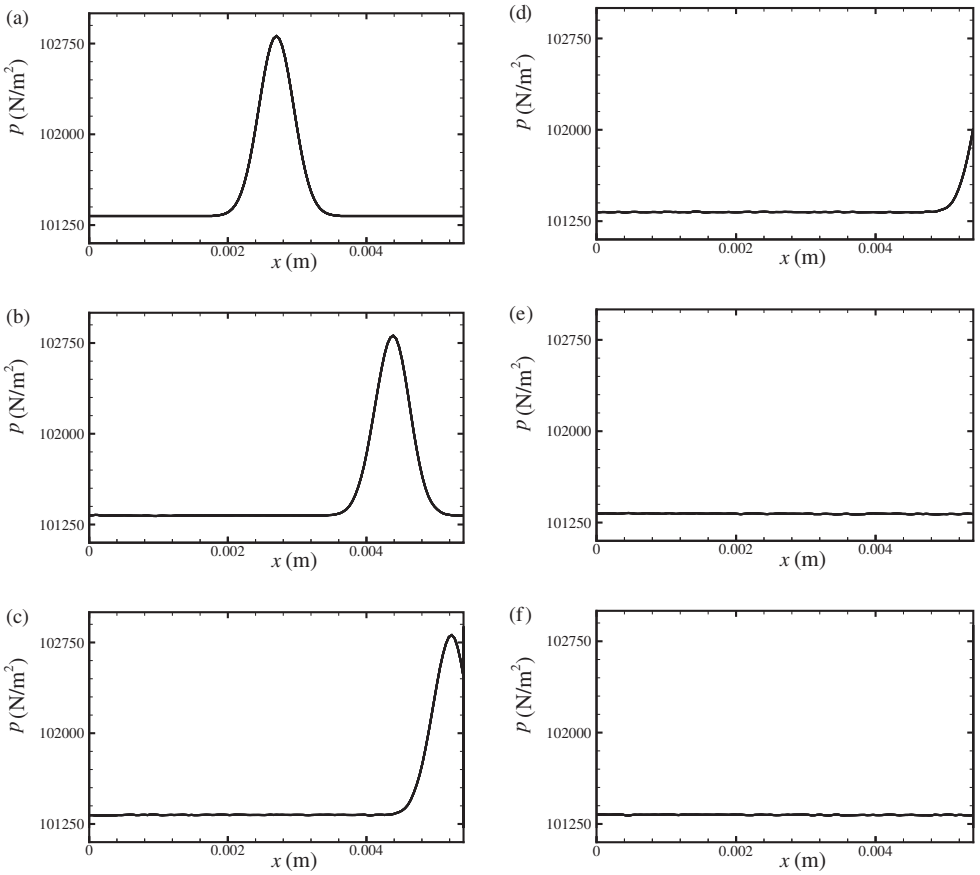

Figure 3. Corresponding pressure ($\mathrm{N\,m^{-2}}$) for case I. In all cases, the scale on the y-axis is unchanged. (*a*) $t_r = 0.0$, (*b*) $t_r = 0.427$, (*c*) $t_r = 0.855$, (*d*) $t_r = 1.068$, (*e*) $t_r = 6.471$, (*f*) $t_r = 12.957$.

domain with no discernable reflections. Case II results are given in figures 4 and 5. Similar to case I, the waves exit the domain without problems. However, inaccuracies are observed a substantially long time after the waves exit the domain. The mean pressure decreases (figures 5(*e*) and (*f*)), while the mean velocity increases (figures 4(*e*) and (*f*)).

4.2. Two-dimensional vortex pair propagation

The boundary condition derivation based on a one-dimensional formulation may lead to inaccuracies in a two-dimensional setting [10, 16]. Therefore, as a two-dimensional representative problem, we generated a pair of counter-rotating vortices on a chemically inhomogeneous, uniform flow u_0 of $25\,\mathrm{m\,s^{-1}}$. The initial velocity components associated with a pair of vortices are generated by using the superimposed stream function ψ [4, 10]

$$u_1 = \frac{\partial \psi}{\partial x_2}, \qquad u_2 = -\frac{\partial \psi}{\partial x_1}, \tag{4.2}$$

where

$$\psi = C \exp\left[-\frac{(x_1 - x_{1v})^2 + (y_1 - y_{1v})^2}{2r_v^2}\right], \tag{4.3}$$

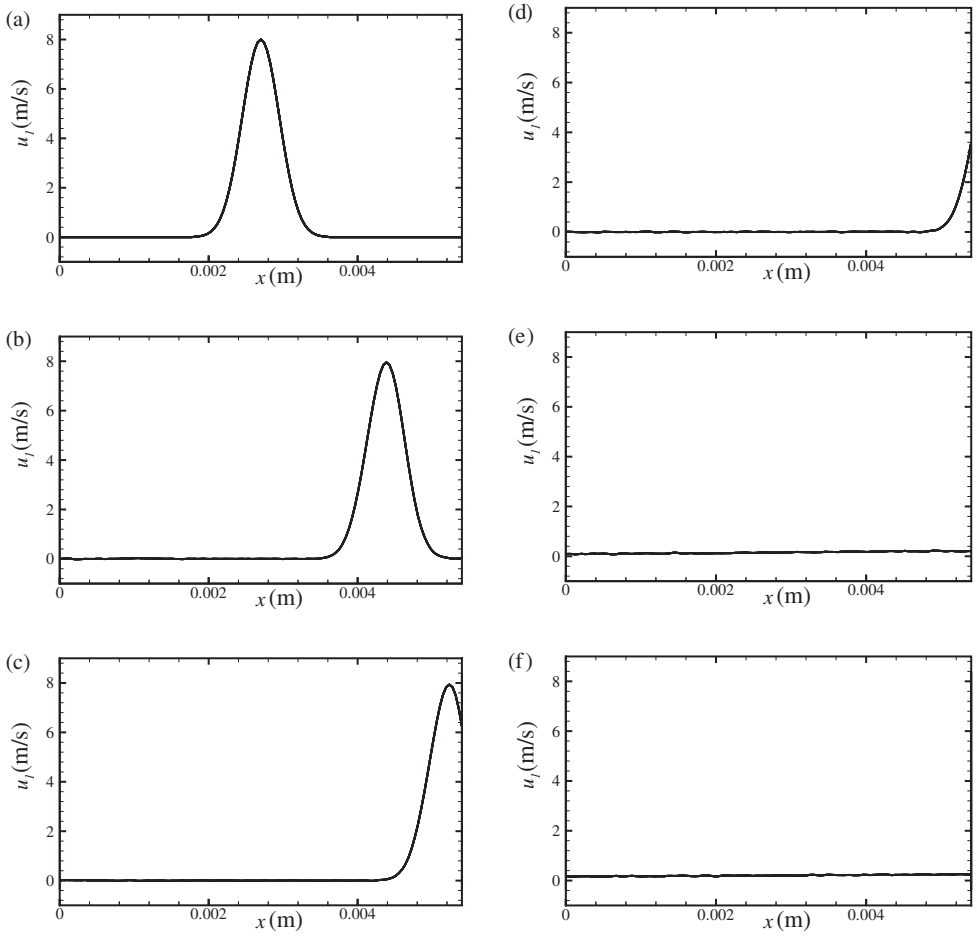

Figure 4. Velocity wave propagation ($\mathrm{m\,s^{-1}}$) for case II. In all cases, the scale on the y-axis is unchanged to facilitate direct comparison. (*a*) $t_r = 0.0$, (*b*) $t_r = 0.427$, (*c*) $t_r = 0.855$, (*d*) $t_r = 1.068$, (*e*) $t_r = 6.471$, (*f*) $t_r = 12.957$.

where x_v and y_v are the coordinates of each vortex centre. The vortex strength is denoted by C. The initial uniform temperature is 300 K. The corresponding initial pressure field is given by [4]

$$p = p_\infty + \rho \frac{C^2}{r_v^2} \exp\left[-\frac{(x_1 - x_{1v})^2 + (y_1 - y_{1v})^2}{r_v^2}\right]. \tag{4.4}$$

The mass fractions of seven species are initialized as shown in figure 1(*b*). The computational domain is 3 cm × 3 cm with a subsonic non-reflecting boundary condition on the lateral boundaries, and a periodic boundary condition at the top and bottom boundaries. The computational domain is discretized by 256 × 256 points.

The results for both cases are plotted from initial time represented by (*a*) and progressively evolve as shown in (*b*)–(*d*). The results at a different value of reduced time $t_r = 2c_0 t/L$, where L is the length of the domain, are shown. Case I results are displayed in figures 6–8. Field variable evolution of vorticity, pressure and Y_{CH_4} is shown, respectively, in figures 6–8. It is found that all the field variables propagate out of the domain with no noticeable numerical reflections. For case II, evolution of vorticity, pressure and Y_{CH_4} is illustrated in figures 9–11,

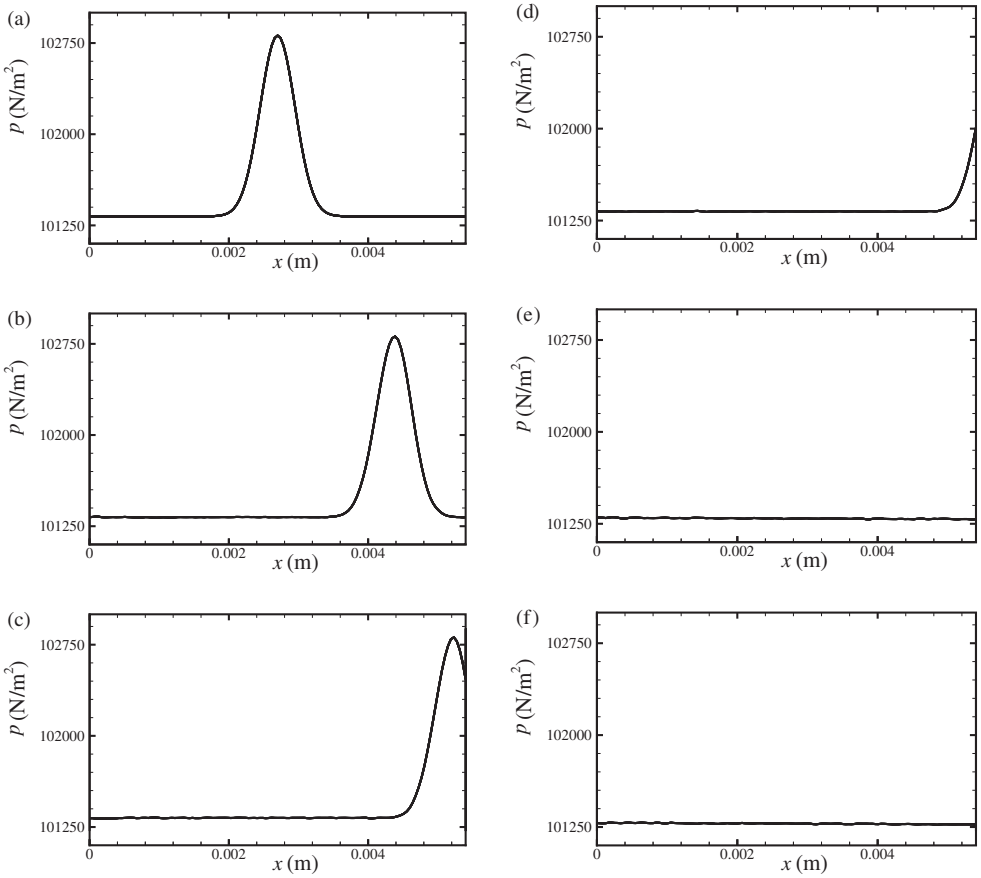

Figure 5. Corresponding pressure ($\mathrm{N\,m^{-2}}$) for case II. In all cases, the scale on the y-axis is unchanged. (*a*) $t_r = 0.0$, (*b*) $t_r = 0.427$, (*c*) $t_r = 0.855$, (*d*) $t_r = 1.068$, (*e*) $t_r = 6.471$, (*f*) $t_r = 12.957$.

respectively. As in case I, vorticity and Y_{CH_4} exit the domain freely. However, it appears that the propagation of vorticity is faster than in case I due to an increase in the mean x-component velocity in the entire domain. The values of velocity become higher than the initial value of the mean uniform flow. This is consistent with the incorrect behaviour observed in the one-dimensional case II in which drift of the mean velocity occurs. Moreover, figure 10(*d*) exhibits perturbations after the vortex exits the domain. Time variations of the instantaneous and the mean pressures are examined at different locations. These locations are shown in figure 11 as indicated by solid circles. Results are depicted in figures 12(*a*) and (*b*) for cases I and II, respectively. Unlike case I, in which overall pressure stays close to atmospheric pressure, in case II the overall pressure decreases throughout the domain during the vortex propagation and continues to decrease after the vortex exits the domain. To gain more insight into these results, the acoustic energy density is considered and is defined by [18, 19]

$$E_D = \frac{p^2}{2\rho c^2} + \frac{\rho(u_1^2 + u_2^2)}{2}, \tag{4.5}$$

where the first term on the right-hand side is the acoustic potential energy density and the second term is the acoustic kinetic energy density. Figure 13 displays time variations of the

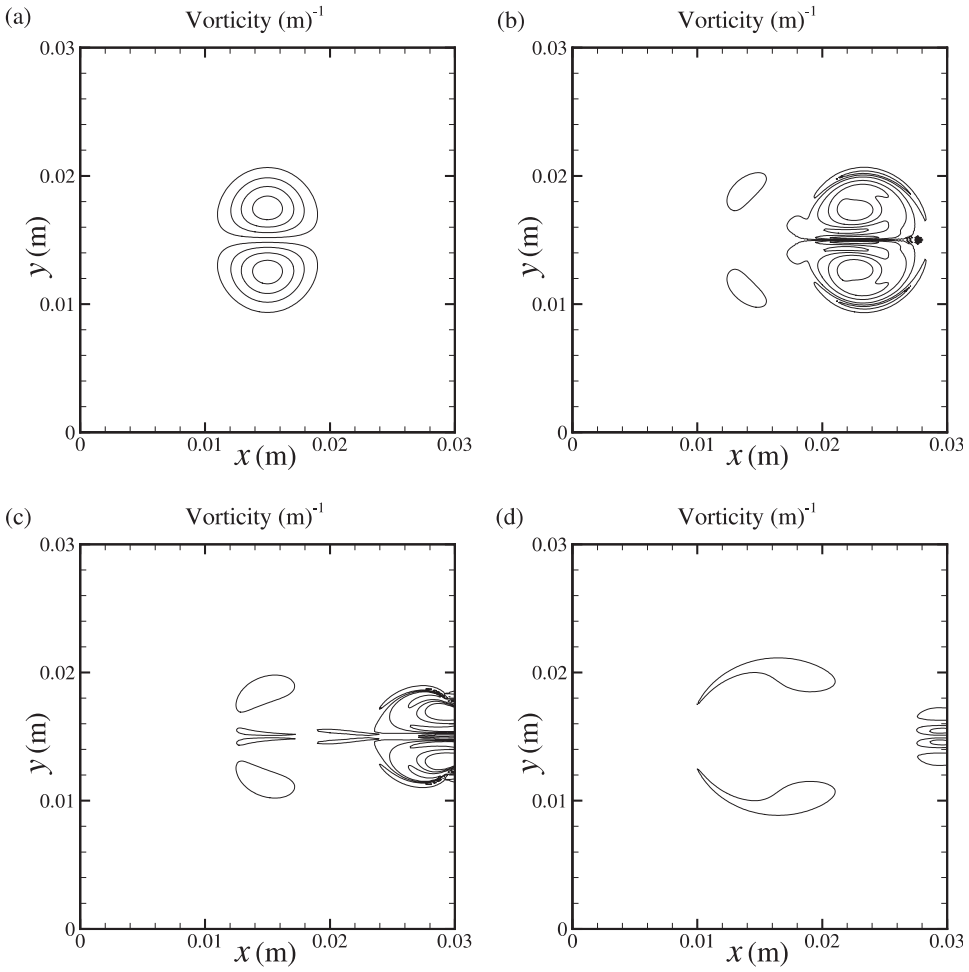

Figure 6. Contours of time evolution of vortex pair for case I. The contours range from −160 000 to 160 000 with 10 equispaced levels. (*a*) $t_r = 0.0$, (*b*) $t_r = 3.0$, (*c*) $t_r = 5.0$, (*d*) $t_r = 12.5$.

acoustic energy density and its two components. Figures 13(*a*)–(*c*), which are for case I, show the acoustic energy density, its potential and kinetic components, respectively. With the same arrangement, figures 13(*d*)–(*f*) represent case II. In this case, the acoustic energy density decreases with time. This result is consistent with the decrease in pressure throughout the simulation time. It is also noted that the overall kinetic acoustic energy density is higher in case II than in case I. This corresponds to the drift of the mean velocity discussed earlier. The inaccurate results are due to inaccuracies in implementing boundary conditions. The results indicate that ignoring the Y_{N_2} contribution to implement boundary conditions leads to unacceptable errors. These errors are suppressed if the species mass fraction gradient at the boundary is zero or very small. The errors become apparent when the mass fraction gradient at the boundary is significant.

4.3. Application to premixed flame

As a final application that includes combustion, the correct treatment of the boundary conditions developed for multicomponent reacting flows is applied to the problem of a counter-rotating

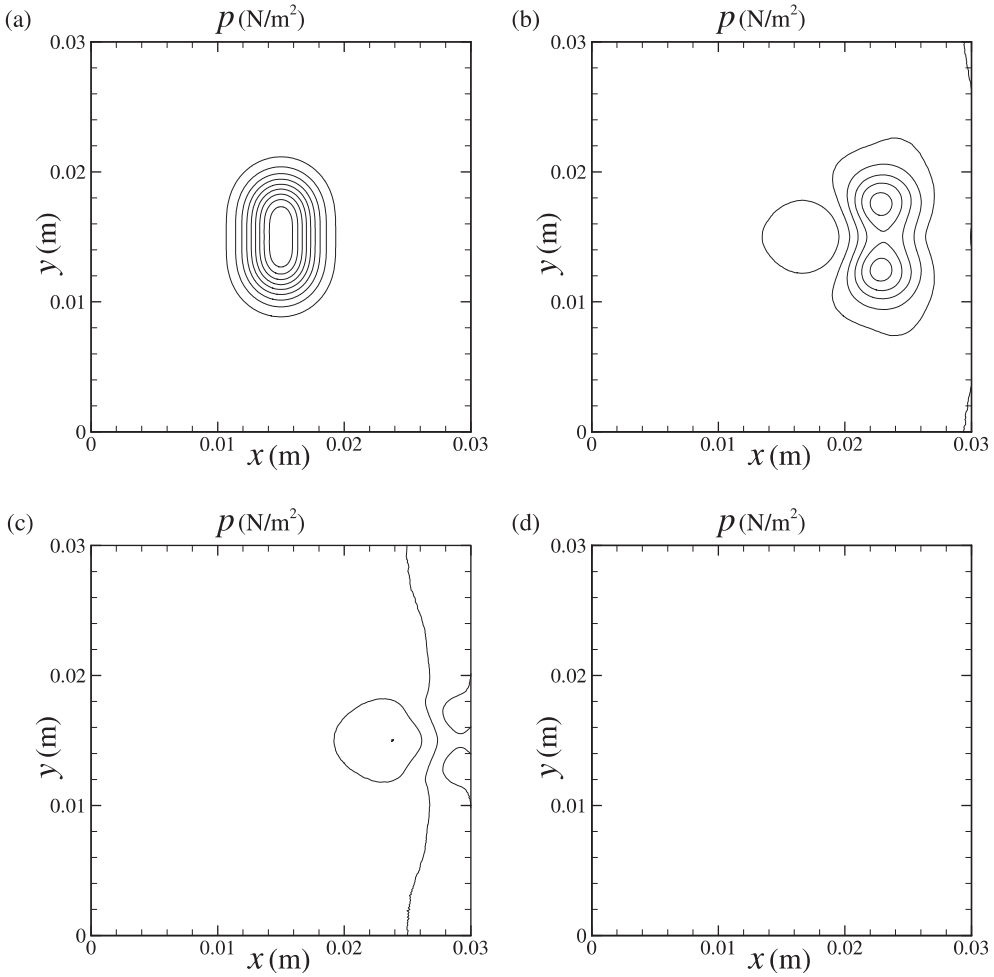

Figure 7. Contours of time evolution of pressure for case I. The contours range from 94 433 to 102 075 with 11 equispaced levels. (*a*) $t_r = 0.0$, (*b*) $t_r = 3.0$, (*c*) $t_r = 5.0$, (*d*) $t_r = 12.5$.

vortex pair interacting with a premixed flame. The fuel utilized is representative of the pyrolysis products of wood. It includes CO, H_2, CH_4 and CO_2. A reduced four-step chemical kinetic scheme is used to model the combustion of pyrolysis gas and air in a premixed flame [20]. A steady one-dimensional laminar premixed flame is computed using CHEMKIN [21]. The mass fractions of the major constituents of the unburnt premixed mixture are $Y_{CO} = 0.082$, $Y_{H_2} = 0.009$, $Y_{CH_4} = 0.014$, $Y_{CO_2} = 0.130$, $Y_{O_2} = 0.178$, and $Y_{N_2} = 0.586$ for an equivalence ratio of unity. The computed flame speed is 65 cm s^{-1} [20]. A pair of counter-rotating vortices generated by using equations (4.2) and (4.3) is initialized in a two-dimensional domain and allowed to interact with the initially planar flame. The 3.0 cm × 3.0 cm domain is discretized using a 360 × 360 uniform grid. The boundary conditions are periodic in the y direction. In the x direction, the subsonic boundary condition is implemented in which the inlet velocity and the temperature are imposed and a non-reflecting boundary condition is prescribed at the outlet. A schematic diagram illustrating the problem is given in figure 14.

The instantaneous data are extracted and investigated. Contours of Y_{CH_4}, Y_{CO_2} and vorticity at the same instant are plotted in figure 15. At this time, the vortex is clearly passing through the

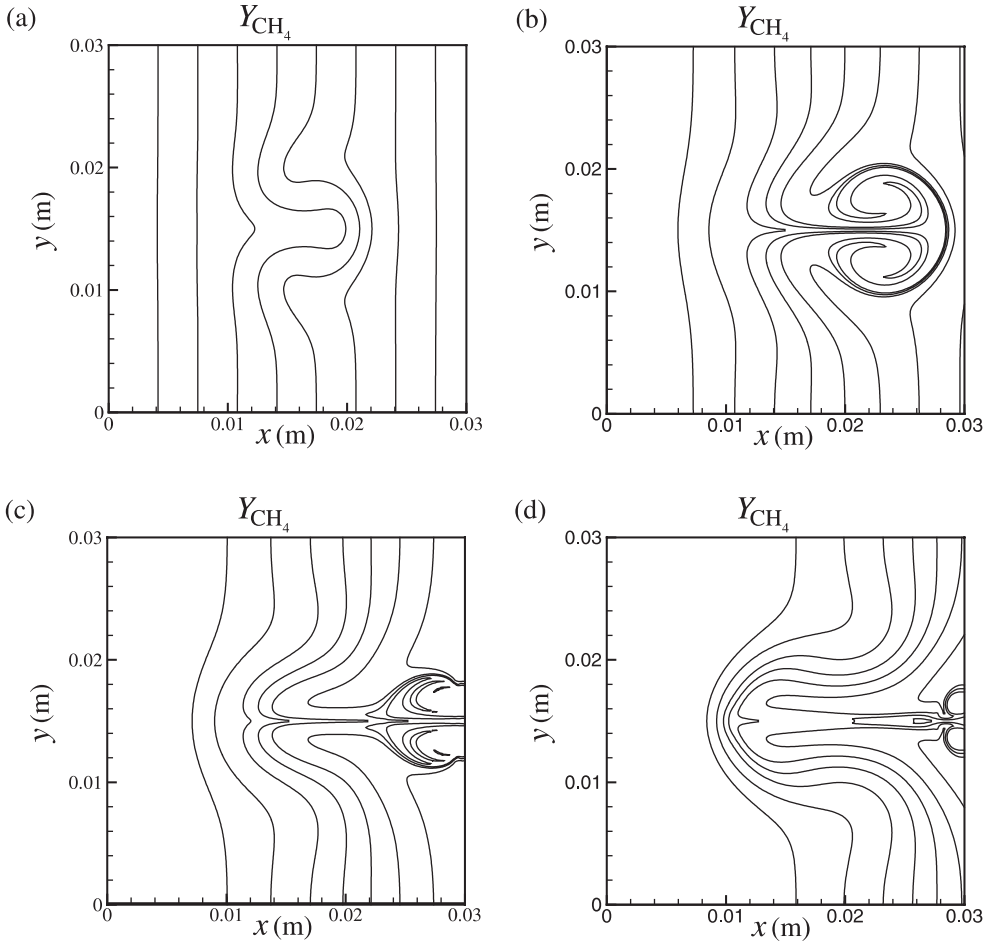

Figure 8. Contours of time evolution of CH_4 mass fraction for case I. The contours range from 0 to 0.2 with 10 equispaced levels. (*a*) $t_r = 0.0$, (*b*) $t_r = 3.0$, (*c*) $t_r = 5.0$, (*d*) $t_r = 12.5$.

exit boundary. Figure 15(*a*) shows contours of Y_{CH_4} and Y_{CO_2}. As CH_4 is completely consumed within the reaction zone, its gradient remains zero at the outflow boundary. On the other hand, non-zero gradients of the primary combustion product Y_{CO_2} are evident at the exit plane. Therefore, this situation represents an appropriate application for testing boundary conditions. The vortex shown in figure 15(*b*) exits the domain smoothly without wave reflections. It travels without creating perturbations during the vortex propagation within the domain as well as after the vortex exits the domain.

5. Conclusions

An accurate method to specify boundary conditions based on characteristic wave analysis for gaseous reacting flows with realistic thermodynamic properties is presented. The formulation of the boundary treatment is derived from a set of primitive variables different from those previously published [9]. Different forms of conservative system, primitive system as well as the LODI relations are obtained. The system of governing equations is rewritten into

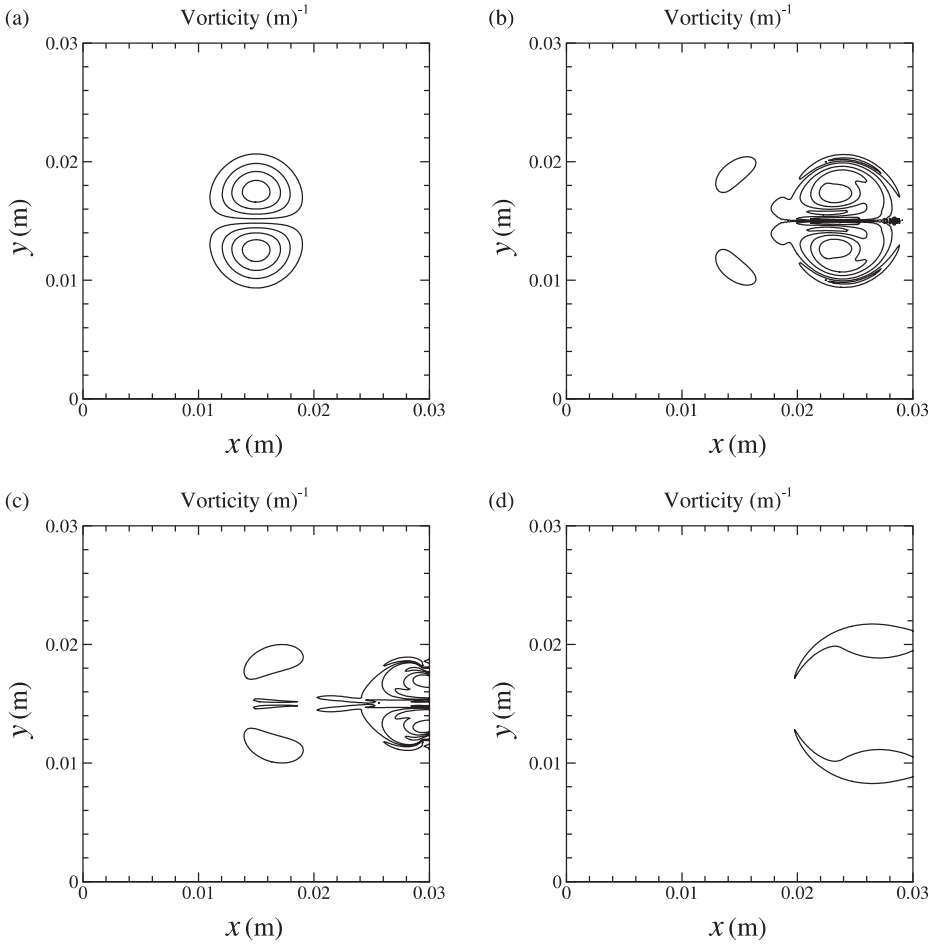

Figure 9. Contours of time evolution of vortex pair for case II. The contours range from −160 000 to 160 000 with 10 equispaced levels. (*a*) $t_r = 0.0$, (*b*) $t_r = 3.0$, (*c*) $t_r = 5.0$, (*d*) $t_r = 12.5$.

characteristic form in which different waves crossing the boundaries can be analysed. Numerical boundary conditions in the form of characteristic waves are specified by considering the LODI relations.

A characteristic wave analysis previously developed to specify boundary conditions for inhomogeneous flows with realistic thermodynamic properties is derived with an alternative set of primitive variables. In a multicomponent reacting flow, it is sufficient to consider the time-integration of all species' mass fractions, excluding one. This work considers excluding the N_2 mass fraction from time-integration. Instead, the mass fraction of N_2 is computed by the constraint that summation of all species' mass fractions is unity. This results in a primitive variable vector that contains one element less. The impact of this choice on the resulting characteristic equations and treatment of numerical boundary conditions are derived and assessed.

The improved accuracy in the treatment of boundary conditions is assessed via three test problems. A one-dimensional test problem involving acoustic wave propagation in a non-uniform mixture of gases is investigated. Following this, a two-dimensional test problem of a counter-rotating vortex pair convecting through a non-uniform mixture of gases is studied.

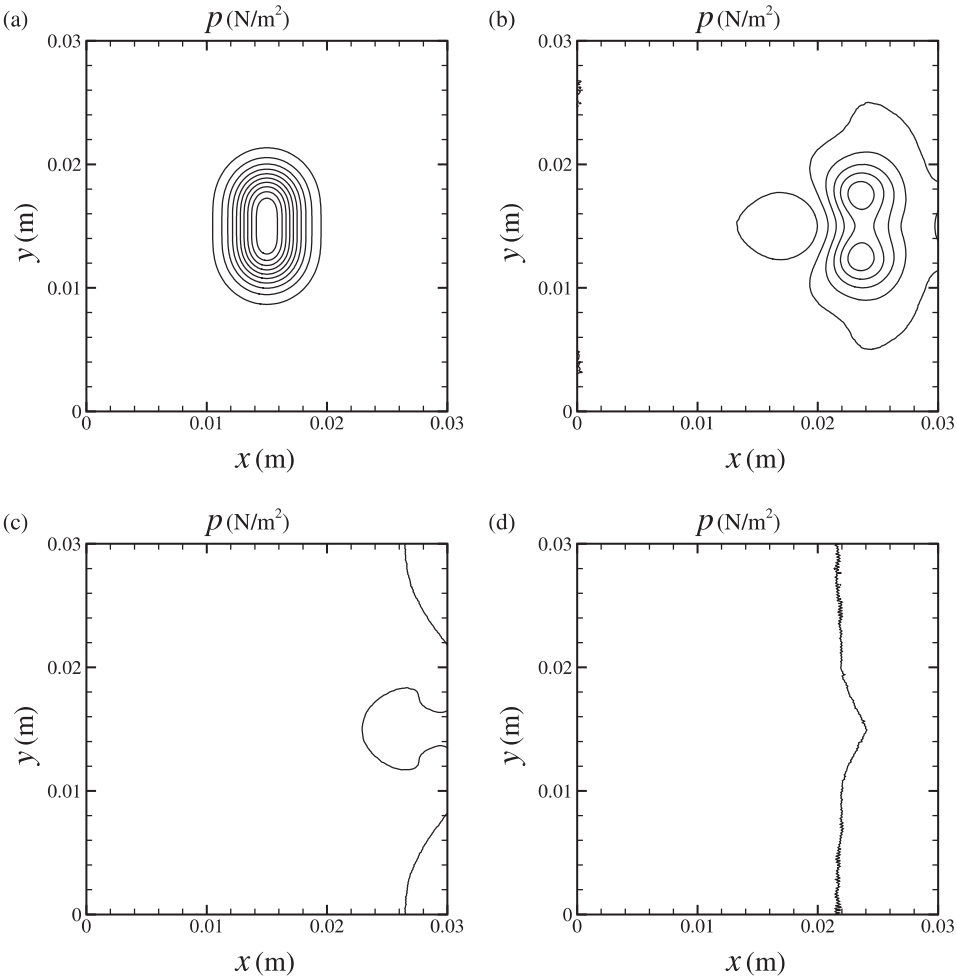

Figure 10. Contours of time evolution of pressure for case II. The contours range from 94 433 to 102 075 with 11 equispaced levels. (*a*) $t_r = 0.0$, (*b*) $t_r = 3.0$, (*c*) $t_r = 5.0$, (*d*) $t_r = 12.5$.

The third problem chosen involves combustion representing the interaction of a counter-rotating vortex pair and a premixed flame. The method is found to treat the boundary conditions accurately as the waves and vortex exit the domain without any significant reflection. Furthermore, the method eliminates drift of the mean pressure that tends to occur over long integration times when the boundary is treated inaccurately. A formulation that neglects the modifications discussed in this paper leads to inaccuracies both in the vicinity of the boundary and the rest of the computational domain. The mathematical formulation reveals that the inaccuracies are naturally suppressed if the mass fraction gradients and/or velocity at the boundary is zero.

Acknowledgments

This material is based upon work supported by the National Science Foundation under Grant No 0049007 for which the authors are grateful. WP is grateful for scholarship support provided by the Royal Thai Government.

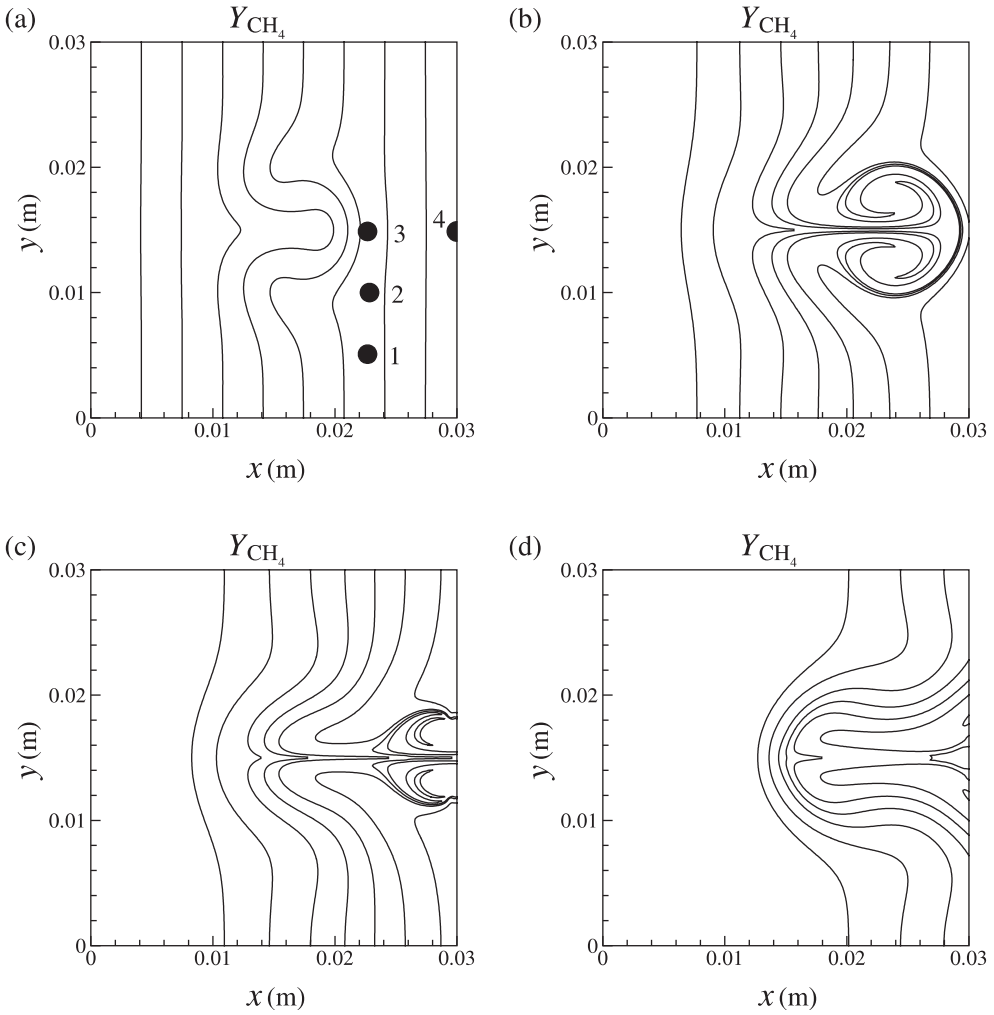

Figure 11. Contours of time evolution of CH_4 mass fraction for case II. The contours range from 0 to 0.2 with 10 equispaced levels. (*a*) $t_r = 0.0$, (*b*) $t_r = 3.0$, (*c*) $t_r = 5.0$, (*d*) $t_r = 12.5$.

Appendix. Derivation for characteristic form of Navier–Stoke equations

The fundamental procedure is based on characteristic wave analysis for Euler equations presented by Thompson [1, 5]. Let U be a vector of time-dependent primitive variables and $\tilde{U}$ correspond to a vector of time-dependent conservative variables. Navier–Stokes equations can be reduced to Euler equations by neglecting viscous terms. The system of equations can be written in vector form as

$$\frac{\partial \tilde{U}}{\partial t} + \frac{\partial F^1}{\partial x_1} + \frac{\partial F^2}{\partial x_2} + \frac{\partial F^3}{\partial x_3} + \tilde{D} = 0, \tag{A.1}$$

where F^k is the flux vector in the k coordinate direction. Vector $\tilde{D}$ contains terms which do not contain any spatial derivatives of U components.

In what follows we consider characteristic analysis in the x_1 direction. Thus, all terms not involving derivatives of $\tilde{U}_i$ in the x_1 direction are grouped together. Equation (A.1) can be

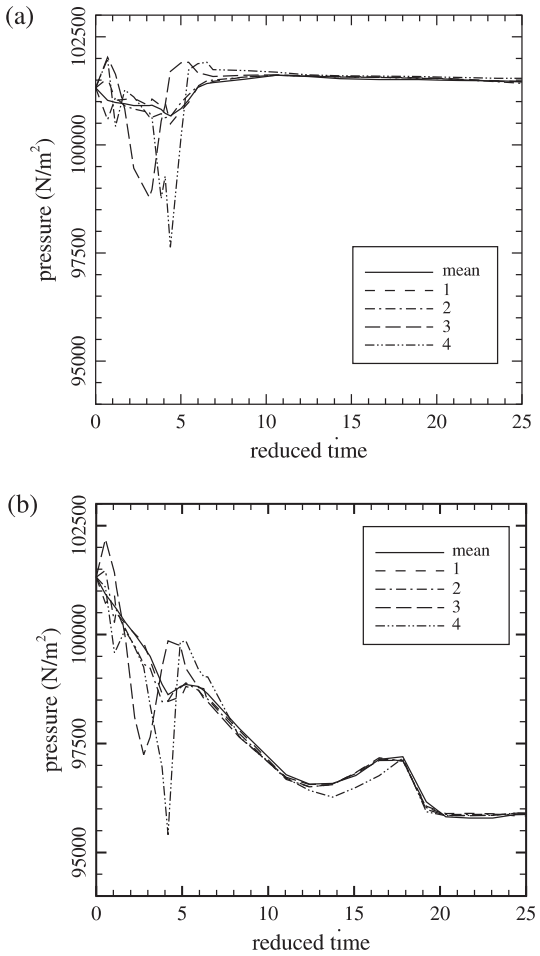

Figure 12. Time variations of the mean and instantaneous pressures at different locations in the domain for case I (*a*) and case II (*b*). The locations are indicated in figure 11.

written as

$$\frac{\partial \tilde{U}}{\partial t} + \frac{\partial F^1}{\partial x_1} + \tilde{C} = 0, \qquad \tilde{C} = \frac{\partial F^2}{\partial x_2} + \frac{\partial F^3}{\partial x_3} + \tilde{D}. \tag{A.2}$$

We form

$$\frac{\partial \tilde{U}}{\partial t} = P \frac{\partial U}{\partial t}, \tag{A.3}$$

where P is a Jacobian matrix whose ith row, jth column element

$$p_{ij} = \frac{\partial \tilde{U}_i}{\partial U_j}. \tag{A.4}$$

We can also form

$$\frac{\partial F^1}{\partial x_1} = Q^1 \frac{\partial U}{\partial x_1}, \tag{A.5}$$

where Q^1 has elements

$$q^1_{ij} = \frac{\partial F^1_i}{\partial U_j}, \tag{A.6}$$

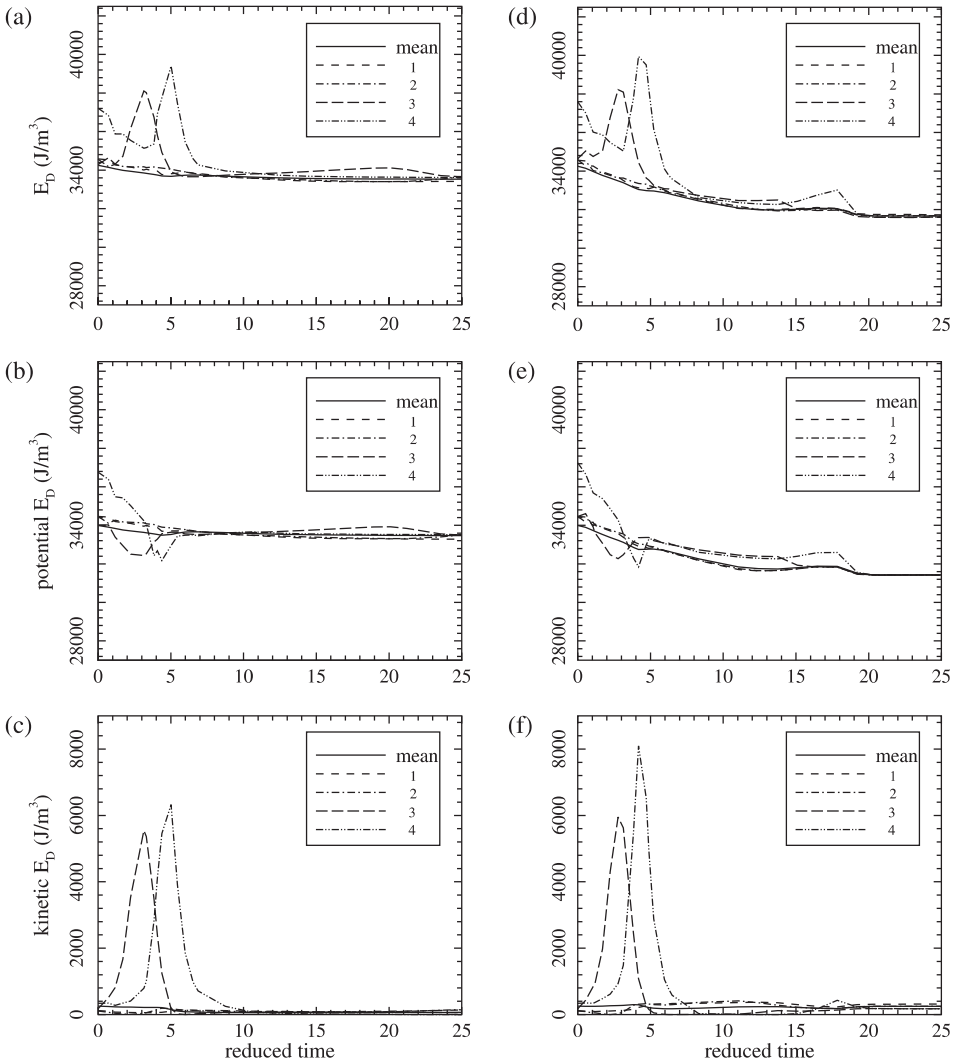

Figure 13. Time variations of the mean and instantaneous acoustic energy densities: total (*a*) and (*d*), potential (*b*) and (*e*), kinetic (*c*) and (*f*) at different locations for case I (*a*)–(*c*) and case II (*d*)–(*f*). The locations are indicated in figure 11.

Premultiplying (A.2) by P^{-1}, the primitive form becomes

$$\frac{\partial U}{\partial t} + A^1 \frac{\partial U}{\partial x_1} + A^2 \frac{\partial U}{\partial x_2} + A^3 \frac{\partial U}{\partial x_3} + D = 0 \tag{A.7}$$

or

$$\frac{\partial U}{\partial t} + A^1 \frac{\partial U}{\partial x_1} + C = 0, \qquad C = A^2 \frac{\partial U}{\partial x_2} + A^3 \frac{\partial U}{\partial x_3} + D, \tag{A.8}$$

where

$$A^k = P^{-1} Q^k, \qquad C = P^{-1} \tilde{C}, \qquad D = P^{-1} \tilde{D}. \tag{A.9}$$

In terms of S whose columns are the right eigenvectors of A^1, (A.8) is recast as

$$\frac{\partial U}{\partial t} + S\mathcal{L} + C = 0, \tag{A.10}$$

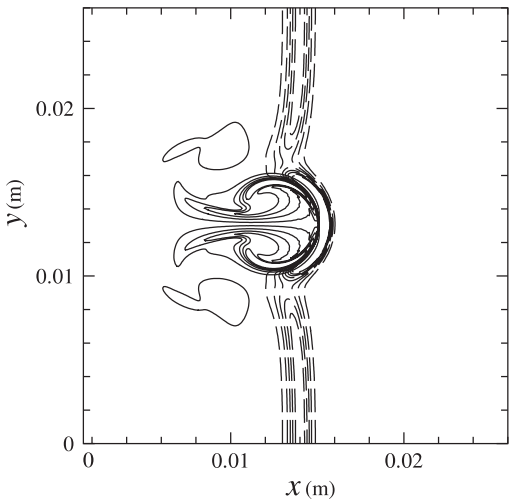

Figure 14. Schematic of two-dimensional premixed flame–vortex interaction. Shown are equispaced contours of vorticity (——) and reaction rate of methane (- - - -). The vortex pair travels to the right. The planar premixed flame speed is 65 cm s^{-1} for an equivalence ratio of unity.

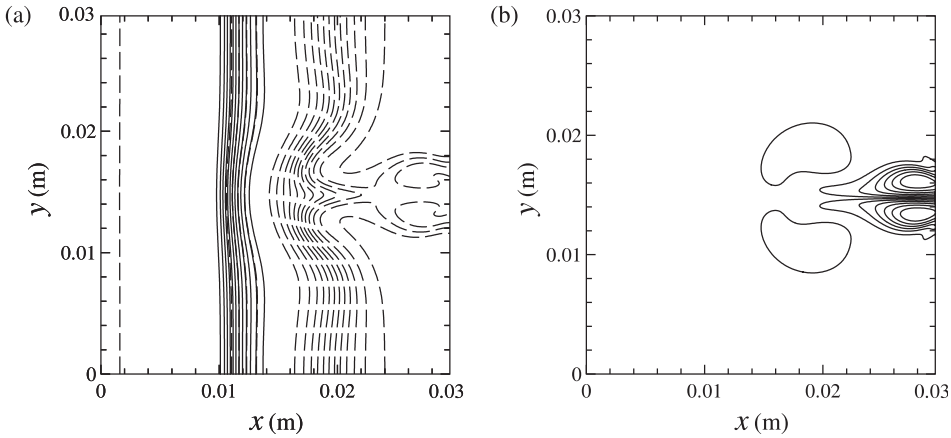

Figure 15. Contours of (*a*) mass fractions of CH_4 (——) and CO_2 (- - - -) and (*b*) contour of vorticity. With 12 equispaced levels, contours of Y_{CH_4} and Y_{CO_2} range from 0.002 to 0.015 and from 0.04 to 0.14, respectively. Vorticity contour ranges from −39 734 to 39 734 with 12 equispaced levels.

where the vector $\mathcal{L}$ has components of characteristic wave amplitudes $\mathcal{L}_i$ defined as

$$\mathcal{L}_i = \lambda_i l_i^{\mathrm{T}} \frac{\partial U}{\partial x_1}, \qquad i = 1, \ldots, m, \tag{A.11}$$

where m is the number of primitive variables. In conservative form the system of equations becomes

$$\frac{\partial \tilde{U}}{\partial t} + PS\mathcal{L} + \tilde{C} = 0. \tag{A.12}$$

For our system of equations which includes continuity, Navier–Stokes, energy and species equations, conservative variables are written in vector form as

$$\tilde{U} = (\rho, \rho e_t, \rho u_1, \rho u_2, \rho u_3, \rho Y_1, \ldots, \rho Y_N)^{\mathrm{T}}. \tag{A.13}$$

The flux vector is given by

$$F^1 = (\rho u_1, (\rho e_t + p)u_1, \rho u_1^2 + p, \rho u_1 u_2, \rho u_1 u_3, \rho u_1 Y_1, \ldots, \rho u_1 Y_N)^{\mathrm{T}}. \tag{A.14}$$

The vector of primitive variables chosen corresponds to

$$U = (\rho, p, u_1, u_2, u_3, Y_1, \ldots, Y_N)^{\mathrm{T}}. \tag{A.15}$$

The Jacobian matrix P constructed by (A.4) is

$$P = \begin{bmatrix} 1 & 0 & 0 & 0 & 0 & 0 & \cdots & \cdots & \cdots & 0 \\ P_{2,1} & P_{2,2} & \rho u_1 & \rho u_2 & \rho u_3 & P_{2,6} & P_{2,7} & \cdots & \cdots & P_{2,N+5} \\ u_1 & 0 & \rho & 0 & 0 & 0 & 0 & \cdots & \cdots & 0 \\ u_2 & 0 & 0 & \rho & 0 & 0 & 0 & \cdots & \cdots & 0 \\ u_3 & 0 & 0 & 0 & \rho & 0 & 0 & \cdots & \cdots & 0 \\ Y_1 & 0 & 0 & 0 & 0 & \rho & 0 & \cdots & \cdots & 0 \\ Y_2 & 0 & 0 & 0 & 0 & 0 & \rho & 0 & \cdots & 0 \\ \vdots & \vdots & \vdots & \vdots & \vdots & \vdots & \ddots & \ddots & \ddots & \vdots \\ Y_{N-1} & 0 & 0 & 0 & 0 & \cdots & \cdots & 0 & \rho & 0 \\ Y_N & 0 & 0 & 0 & 0 & 0 & \cdots & \cdots & 0 & \rho \end{bmatrix}, \tag{A.16}$$

where elements

$$P_{2,1} = \frac{1}{2} u_k u_k + \sum_{\kappa=1}^{N} Y_\kappa h_\kappa - \bar{C}_p T, \tag{A.17}$$

$$P_{2,2} = \frac{\bar{C}_p}{R} - 1, \tag{A.18}$$

$$P_{2,\kappa+5} = \rho h_\kappa - \sum_{\kappa'=1}^{N} p \frac{\bar{W}}{W_\kappa} Y_{\kappa'} \frac{C_{p,\kappa'}}{R}, \qquad \kappa = 1, \ldots, N. \tag{A.19}$$

Then we may compute P^{-1}, which is given by

$$P^{-1} = \begin{bmatrix} 1 & 0 & 0 & 0 & 0 & 0 & \cdots & \cdots & \cdots & 0 \\ P_{2,1}^{-1} & \dfrac{1}{P_{2,2}} & \dfrac{-u_1}{P_{2,2}} & \dfrac{-u_2}{P_{2,2}} & \dfrac{-u_3}{P_{2,2}} & P_{2,6}^{-1} & P_{3,6}^{-1} & \cdots & \cdots & P_{2,N+5}^{-1} \\ \dfrac{-u_1}{\rho} & 0 & \dfrac{1}{\rho} & 0 & 0 & 0 & 0 & \cdots & \cdots & 0 \\ \dfrac{-u_2}{\rho} & 0 & 0 & \dfrac{1}{\rho} & 0 & 0 & 0 & \cdots & \cdots & 0 \\ \dfrac{-u_3}{\rho} & 0 & 0 & 0 & \dfrac{1}{\rho} & 0 & 0 & \cdots & \cdots & 0 \\ \dfrac{-Y_1}{\rho} & 0 & 0 & 0 & 0 & \dfrac{1}{\rho} & 0 & \cdots & \cdots & 0 \\ \dfrac{-Y_2}{\rho} & 0 & 0 & 0 & 0 & 0 & \dfrac{1}{\rho} & 0 & \cdots & 0 \\ \vdots & \vdots & \vdots & \vdots & \vdots & \vdots & \ddots & \ddots & \ddots & \vdots \\ \dfrac{-Y_{N-1}}{\rho} & 0 & 0 & 0 & 0 & \cdots & \cdots & 0 & \dfrac{1}{\rho} & 0 \\ \dfrac{-Y_N}{\rho} & 0 & 0 & 0 & 0 & 0 & \cdots & \cdots & 0 & \dfrac{1}{\rho} \end{bmatrix}, \tag{A.20}$$

where elements

$$P_{2,1}^{-1} = \frac{-P_{2,1} + u_k u_k + \sum_{\kappa=1}^{N} Y_\kappa (h_\kappa - \sum_{\kappa'=1}^{N} (p/\rho R)(\bar{W}/W_\kappa) Y_{\kappa'} C_{p,\kappa'})}{P_{2,2}}, \tag{A.21}$$

$$P_{2,\kappa+5}^{-1} = \frac{\sum_{\kappa'=1}^{N} (p/\rho R)(\bar{W}/W_\kappa) Y_{\kappa'} C_{p,\kappa'} - h_\kappa}{P_{2,2}}, \qquad \kappa = 1, \ldots, N. \tag{A.22}$$

Subsequently, matrix Q^1 given by (A.6) can be written as

$$Q^1 = \begin{bmatrix} u_1 & 0 & \rho & 0 & 0 & 0 & \cdots & \cdots & 0 \\ P_{2,1}u_1 & Q_{2,2}^1 & Q_{2,3}^1 & \rho u_1 u_2 & \rho u_1 u_3 & Q_{2,6}^1 & \cdots & \cdots & Q_{2,N+5}^1 \\ u_1^2 & 1 & 2\rho u_1 & 0 & 0 & 0 & \cdots & \cdots & 0 \\ u_1 u_2 & 0 & \rho u_2 & \rho u_1 & 0 & 0 & \cdots & \cdots & 0 \\ u_1 u_3 & 0 & \rho u_3 & 0 & \rho u_1 & 0 & \cdots & \cdots & 0 \\ u_1 Y_1 & 0 & \rho Y_1 & 0 & 0 & \rho u_1 & 0 & \cdots & 0 \\ u_1 Y_2 & 0 & \rho Y_2 & 0 & 0 & 0 & \ddots & \cdots & 0 \\ \vdots & \vdots & \vdots & \vdots & \vdots & \vdots & \ddots & \ddots & \vdots \\ u_1 Y_N & 0 & 0 & \rho Y_N & 0 & 0 & \cdots & 0 & \rho u_1 \end{bmatrix}, \tag{A.23}$$

where elements

$$Q_{2,2}^1 = (P_{2,2} + 1)u_1, \tag{A.24}$$

$$Q_{2,3}^1 = (\rho e_t + p) + \rho u_1^2, \tag{A.25}$$

$$Q_{2,\kappa+5}^1 = u_1 \left(\rho h_\kappa - \sum_{\kappa'=1}^{N} p \frac{\bar{W}}{W_\kappa} Y_{\kappa'} \frac{C_{p,\kappa'}}{R} \right), \qquad \kappa = 1, \ldots, N. \tag{A.26}$$

Following (A.9), matrix A^1 can then be formed and is given by

$$A^{-1} = \begin{bmatrix} u_1 & 0 & \rho & 0 & 0 & 0 & \cdots & \cdots & \cdots & 0 \\ 0 & u_1 & p\left(\dfrac{\bar{C}_p}{\bar{C}_p - R}\right) & 0 & 0 & 0 & 0 & \cdots & \cdots & 0 \\ 0 & \dfrac{1}{\rho} & u_1 & 0 & 0 & 0 & 0 & \cdots & \cdots & 0 \\ 0 & 0 & 0 & u_1 & 0 & 0 & 0 & \cdots & \cdots & 0 \\ 0 & 0 & 0 & 0 & u_1 & 0 & 0 & \cdots & \cdots & 0 \\ 0 & 0 & 0 & 0 & 0 & u_1 & 0 & \cdots & \cdots & 0 \\ 0 & 0 & 0 & 0 & 0 & 0 & u_1 & 0 & \cdots & 0 \\ \vdots & \vdots & \vdots & \vdots & \vdots & \vdots & \ddots & \ddots & \ddots & \vdots \\ 0 & 0 & 0 & 0 & 0 & \cdots & \cdots & \cdots & u_1 & 0 \\ 0 & 0 & 0 & 0 & 0 & 0 & \cdots & \cdots & 0 & u_1 \end{bmatrix}. \tag{A.27}$$

Primitive equations can then be formed as in (A.8) with the eigenvalues of A^1:

$$\begin{aligned}
\lambda_1 &= u_1 - c,\\
\lambda_2 &= u_1,\\
\lambda_3 &= u_1,\\
\lambda_4 &= u_1,\\
\lambda_5 &= u_1 + c,\\
\lambda_6 &= u_1,\\
\vdots &= \vdots\\
\lambda_{N+5} &= u_1,
\end{aligned} \tag{A.28}$$

where c is the speed of sound in the reacting gas mixture, defined as

$$c = \sqrt{\gamma RT}. \tag{A.29}$$

The specific heat ratio γ in (A.29) is given by

$$\gamma = \frac{\bar{C}_p}{\bar{C}_p - R}. \tag{A.30}$$

The corresponding left eigenvectors of dimension $1 \times (N + 5)$ are

$$\begin{aligned}
l_1^{\mathrm{T}} &= (0, 1, -\rho c, 0, 0, \ldots, 0),\\
l_2^{\mathrm{T}} &= \left(0, u_1 - c, p\left(\frac{\bar{C}_p}{\bar{C}_p - R}\right) - \quad \rho c u_1, 0, \ldots, 0\right),\\
l_3^{\mathrm{T}} &= (0, 0, 0, 1, 0, 0, \ldots, 0),\\
l_4^{\mathrm{T}} &= (0, 0, 0, 0, 1, 0, \ldots, 0),\\
l_5^{\mathrm{T}} &= (0, 1, \rho c, 0, 0, \ldots, 0),\\
l_6^{\mathrm{T}} &= (0, 0, 0, 0, 0, 1, 0, \ldots, 0),\\
l_7^{\mathrm{T}} &= (0, 0, \ldots, 0, 1, 0, 0, 0, 0),\\
l_8^{\mathrm{T}} &= (0, 0, \ldots, 0, 0, 1, 0, 0, 0),\\
\vdots &= \vdots\\
l_{N+5}^{\mathrm{T}} &= (0, 0, \ldots, 0, 1).
\end{aligned} \tag{A.31}$$

The above eigenvectors are used to define the characteristic wave amplitudes $\mathcal{L}_i$ in (A.11).

References

[1] Thompson K W 1987 Time dependent boundary conditions for hyperbolic systems *J. Comput. Phys.* **68** 1–24

[2] Lele S K 1992 Compact finite difference schemes with spectral-like resolution *J. Comput. Phys.* **103** 16–42

[3] Poinsot T J, Veynante D and Candel S 1991 Quenching processes and premixed turbulent combustion diagrams *J. Fluid Mech.* **228** 561–606

[4] Poinsot T J and Lele S K 1992 Boundary conditions for direct simulations of compressible viscous flows *J. Comput. Phys.* **101** 104–29

[5] Thompson K W 1990 Time-dependent boundary conditions for hyperbolic systems II *J. Comput. Phys.* **89** 439–61

[6] Kreiss H-O 1970 Initial boundary value problems for hyperbolic systems *Commun. Pure Appl. Math.* **23** 277–98

[7] Higdon R 1986 Initial-boundary value problems for linear hyperbolic systems *SIAM Rev.* **28** 177–217

[8] Engquist B and Majda A 1977 Absorbing boundary conditions for numerical simulations of waves *Math. Comput.* **31** 629

[9] Baum M, Poinsot T and Thevenin D 1994 Accurate boundary conditions for multicomponent reactive flows *J. Comput. Phys.* **116** 247–61

[10] Okong'o N and Bellan J 2002 Consistent boundary conditions for multicomponent real gas mixtures based on characteristic waves *J. Comput. Phys.* **176** 330–44
[11] Oliger J and Sundtröm A 1978 Theoretical and practical aspects of some initial boundary value problems in fluid dynamics *SIAM J. Appl. Math.* **35** 419–34
[12] Rudy D H and Strikwerda J C 1980 A nonreflecting outflow boundary condition for subsonic Navier–Stokes calculations *J. Comput. Phys.* **36** 55–70
[13] Rudy D H and Strikwerda J C 1981 Boundary conditions for subsonic compressible Navier–Stokes calculations *Comput. Fluids.* **9** 327–38
[14] Guichard L, Vervisch L and Domingo P 1995 Two dimensional weak-shock vortex interaction in mixing zone *AIAA J.* **33** 10
[15] Smooke M D and Giovangigli V 1991 Reduced kinetic mechanisms for asymptotic approximations for methane–air flames *Lecture Notes in Physics* no **384** (Berlin: Springer) 1
[16] Colonius T, Lele S and Moin P 1993 Boundary conditions for direct computation of aerodynamic sound generation *AIAA J.* **31** 1574–82
[17] Renard P-H, Thévenin D, Rolon J C and Candel S 2000 Dynamics of flame/vortex interactions *Prog. Energy Combust. Sci.* **26** 225–82
[18] Pierce A D 1981 *Acoustics: An Introduction to its Physical Principles and Applications* (New York: McGraw-Hill)
[19] Cazzolato B S and Hansen C H 2000 Errors in the measurement of acoustic energy density in one-dimensional sound fields *J. Sound Vib.* **236** 801–31
[20] Zhou X and Mahalingam S 2001 Evaluation of reduced mechanism for modeling combustion of pyrolysis gas in wildland fire *Combust. Sci. Technol.* **236** 39–70
[21] Kee R J, Rupley F M and Miller J A 1985 CHEMKIN II: a fortran program for modeling steady laminar one-dimensional premixed flames *Sandia Report* SAND85–8240 (Livermore, CA: Sandia National Laboratories)